Understanding the mechanisms of solid-water reactions through analysis of surface topography

Joel Z. Bandstra[1,*] and Susan L. Brantley[2]

[1]*Department of Math, Engineering, and Computer Science, Saint Francis University, P.O. Box 600, Loretto, Pennsylvania 15541, USA*

[2]*Earth and Environmental Systems Institute, and Department of Geosciences, Pennsylvania State University, 2217 EES Building, University Park, Pennsylvania 16802, USA*

(Received 6 June 2015; published 8 December 2015)

The topography of a reactive surface contains information about the reactions that form or modify the surface and, therefore, it should be possible to characterize reactivity using topography parameters such as surface area, roughness, or fractal dimension. As a test of this idea, we consider a two-dimensional (2D) lattice model for crystal dissolution and examine a suite of topography parameters to determine which may be useful for predicting rates and mechanisms of dissolution. The model is based on the assumption that the reactivity of a surface site decreases with the number of nearest neighbors. We show that the steady-state surface topography in our model system is a function of, at most, two variables: the ratio of the rate of loss of sites with two neighbors versus three neighbors (d_2/d_3) and the ratio of the rate of loss of sites with one neighbor versus three neighbors (d_1/d_3). This means that relative rates can be determined from two parameters characterizing the topography of a surface provided that the two parameters are independent of one another. It also means that absolute rates cannot be determined from measurements of surface topography alone. To identify independent sets of topography parameters, we simulated surfaces from a broad range of d_1/d_3 and d_2/d_3 and computed a suite of common topography parameters for each surface. Our results indicate that the fractal dimension D and the average spacing between steps, $E[s]$, can serve to uniquely determine d_1/d_3 and d_2/d_3 provided that sufficiently strong correlations exist between the steps. Sufficiently strong correlations exist in our model system when $D > 1.5$ (which corresponds to $D > 2.5$ for real 3D reactive surfaces). When steps are uncorrelated, surface topography becomes independent of step retreat rate and D is equal to 1.5. Under these conditions, measures of surface topography are not independent and any single topography parameter contains all of the available mechanistic information about the surface. Our results also indicate that root-mean-square roughness cannot be used to reliably characterize the surface topography of fractal surfaces because it is an inherently noisy parameter for such surfaces with the scale of the noise being independent of length scale.

DOI: 10.1103/PhysRevE.92.062114 PACS number(s): 05.50.+q, 64.60.al, 61.43.Hv

I. INTRODUCTION

In a wide variety of physical systems, interfaces are formed and modified by molecular scale processes. Examples include (i) the formation of grain boundaries during solidification from molten metal [1,2], (ii) formation of crystals either by precipitation from oversaturated solutions or by vapor deposition or epitaxy [3,4], (iii) nucleation, aggregation, and growth of polymeric materials [5], (iv) evolution of biofilms on mineral surfaces [6–8], (v) etching of crystalline solids [9,10], and (vi) chemical weathering of alumino-silicate minerals [11–14]. In all of these cases, the physical topography of the interface is a complex function of the nature and frequency of the chemical processes that form or modify it. It should, therefore, be possible to ascertain information about the chemical processes from measurements of the surface topography. This idea has been explored to a limited extent in the literature [15], but, to our knowledge, theory-based guidance on this problem has yet to appear.

The ability to determine information about molecular-scale processes based on surface topography could be especially useful in understanding the rates and mechanisms of chemical weathering of alumino-silicate minerals because these reactions happen so slowly that they often must be studied in the laboratory under conditions that differ significantly from natural systems in temperature, specific surface area, or chemical saturation index [16]. The problems inherent to laboratory-based weathering experiments are exemplified by the so-called lab-field discrepancy, where laboratory measurements of mineral dissolution rates are almost uniformly several orders of magnitude greater than field-based estimates of the same [17]. A surface topography-based method for constraining dissolution rates could be used to estimate the rate constants of dissolution reactions for minerals that have weathered under natural conditions over long periods of time. Such a method might also enable more accurate prediction of natural weathering rates from relatively short-time scale laboratory experiments.

In this paper, we explore the possibility of topography-based constraints on mineral dissolution rates using a simple two-dimensional (2D) mathematical model for dissolution. We have previously used this model to examine the general dependence of mineral dissolution rates on various environmental factors [18]. Others have used essentially the same model to study the distribution of steps and kinks on the surface of growing crystals [19–28] and the movement of dislocations during plastic deformation of ductile solids [29]. We believe that this model occupies a middle ground between being so simple as to be irrelevant to real systems and being so complicated as to preclude mathematical analysis. Furthermore, as shown in our previous contribution [18], such a model can successfully predict certain observed features of dissolution behavior including the length of the transient

*Corresponding author: jbandstra@francis.edu

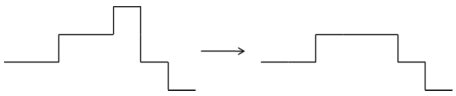

FIG. 1. Example sequence of integer steps that can represent a surface. The reaction from left to right represents dissolution of a site with one nearest neighbor.

period during which rates typically decrease from an initial fast rate to a slower steady-state dissolution rate as well as the behavior of dissolution rate versus free energy of dissolution. A summary description of the model is provided below.

II. MODEL DESCRIPTION

A simple model for a surface embedded in two dimensions is a sequence of steps as shown in Fig. 1. The height of each step is an integer which can be positive, negative, or zero. A positive value indicates a step up going from left to right and a negative value indicates a step down. This model can only represent surfaces with no overhangs. The sequence of step heights for the surface on the left-hand side of Fig. 1 is 0,1,0,1,–2, –1. We define the length L as the lateral extent of the surface so that a surface of length L contains L–1 steps (assuming unit length between steps). Both of the surfaces shown in Fig. 1 have $L = 7$. As discussed later, however, the surface areas of the two examples are different.

Dissolution and precipitation reactions can be incorporated into the model by allowing the values of two neighboring step heights to change concurrently. For a dissolution reaction, the left-hand member of the pair decreases by one and the right-hand member increases by one. For precipitation, the opposite changes occur. The reaction depicted in Fig. 1 (from left to right) is a dissolution reaction between the fourth and fifth steps: 0, 1, 0, 1, –2, –1 → 0, 1, 0, 0, –1, –1.

Like all chemical reactions, dissolution and precipitation are stochastic processes and, therefore, the surfaces formed by these reactions are also stochastic [20–22]. The stochastic nature of the surface can be accounted for in the 2D step model by defining a probability for each possible sequence of steps. Unless the surface is in a steady-state configuration, dissolution and precipitation reactions will change the step sequence probabilities over time. The probability associated with the sequence shown in Fig. 1 can be denoted as $P_t(n_1,n_2,n_3,n_4,n_5,n_6)$.

If the step heights are uncorrelated, then the surface can be described by specifying the probability $P_t(n)$ of observing a step of height n at a randomly selected location and at time t. For uncorrelated steps, the probability of a sequence of steps is equal to the product of the probabilities for the individual step heights, e.g., $P_t(n_1,n_2,n_3,n_4,n_5,n_6) = P_t(n_1)P_t(n_2)P_t(n_3)P_t(n_4)P_t(n_5)P_t(n_6)$.

Chemical reactions can be modeled as Markov chains [30]. For the 2D step model, this means that the time rate of change of the $P_t(n_1,n_2,n_3,n_4,n_5,n_6,\ldots)$ depends only on the current state of the surface. The full dynamics of the surface can be specified via the transition probabilities between each possible sequence of steps. Since the reactions can be treated as occurring one at a time [31], the transition probabilities between most surfaces are zero. This, however, still leaves a very large number of nonzero transition probabilities, particularly for surfaces with large values of L.

The stochastic model can be simplified by supposing that the reaction frequencies are uniquely determined by the configuration of the surface around each reaction site—i.e., the site neighborhood or the short-range ordering of the solid phase. In this context, a reaction site is a region of the surface between two steps where a dissolution or precipitation reaction can occur. To this end, let d_N and p_N denote the probability per unit time of, respectively, dissolution and precipitation at sites with N occupied nearest neighbors. For surfaces with no overhangs such as that shown in Fig. 1, the number of nearest neighbors, N, can take values of 1, 2, or 3 and is determined by the step heights to the left and right of the site. For dissolution,

$$d(n_L,n_R) = \begin{cases} d_1 & n_L > 0 \quad \text{and} \quad n_R < 0 \\ d_3 & n_L \leqslant 0 \quad \text{and} \quad n_R \geqslant 0 \\ d_2 & \text{else,} \end{cases} \tag{1}$$

where n_L and n_R are, respectively, the step heights to the left and right of the dissolution site. A slightly modified version of Eq. (1) can be written for precipitation.

For the remainder of this work, precipitation reactions will be ignored (i.e., $p_N = 0$). The master equation can then be written as

$$\begin{aligned} &\frac{dP_t(n_1\ldots n_{i-1},n_i\ldots n_{L-1})}{dt} \\ &= \sum_{i=2}^{L-1} d(n_{i-1}+1,n_i-1)P_t(n_1\ldots n_{i-1}+1,n_i-1\ldots n_{L-1}) \\ &\quad - \sum_{i=2}^{L-1} d(n_{i-1},n_i)P_t(n_1\ldots n_{i-1},n_i\ldots n_{L-1}), \end{aligned} \tag{2}$$

where $d(n_{i-1},n_i)$ is the probability of dissolution per unit time as defined by Eq. (1) and the summations run over all possible dissolution reaction sites. Ignoring precipitation is equivalent to restricting our view to far-from-equilibrium conditions. While precipitation reactions do influence the development of surface topography [12], the far-from-equilibrium case is of greatest interest because many geologic specimens weather under such conditions and because most laboratory experiments have been conducted far from equilibrium. Focusing on dissolution reactions alone decreases the degrees of freedom in our model to two (see below), allowing simulation results to be presented graphically.

Numerous computational studies of the model described above [18,21,29] and related models [13,24,28,32–36] have identified apparent steady-state behavior for a wide variety of the d_N and p_N. Moreover, an approximate steady-state solution to the master equation can be found by assuming no correlation between step heights at different locations [18,20–22]. The simulations presented in this study were performed for a length of time shown to be sufficient to remove any time-varying component (see below) and, therefore, the results presented are intended to represent the steady-state configuration of the surface. A steady-state surface for real minerals would presumably be represented by a crystal dissolving in a flowing fluid whose chemistry was maintained constant in time, i.e.,

a mineral weathering in an aquifer or soil profile under conditions of flowing ground or pore water maintained at constant chemistry.

At steady state, the time derivative on the left-hand side of Eq. (2) is zero. All of the remaining terms can then be divided by one of the dissolution probabilities per unit time, say, d_3. Equation (2) then becomes

$$0 = \sum_{i=2}^{L-1} \frac{d(n_{i-1}+1, n_i-1)}{d_3} P_{SS}(n_1 \ldots n_{i-1}+1, n_i-1 \ldots n_{L-1}) - \sum_{i=2}^{L-1} \frac{d(n_{i-1}, n_i)}{d_3} P_{SS}(n_1 \ldots n_{i-1}, n_i \ldots n_{L-1}). \quad (3)$$

The only model parameters that appear in Eq. (3) are the ratio of dissolution probabilities, d_1/d_3 and d_2/d_3. Therefore, the steady-state configuration of the surface depends only on these two degrees of freedom.

To our knowledge, a general solution to Eq. (3) has not been found. An approximate solution can be found by assuming that the surface steps are uncorrelated [18,21,22]:

$$P_{SS}(n) = \frac{\sqrt{d_1/d_3}-1}{\sqrt{d_1/d_3}+1} (\sqrt{d_1/d_3})^{-|n|}. \quad (4)$$

The assumption of uncorrelated steps is, however, appropriate only under certain conditions [20]. The exact nature of these conditions is discussed further below. In those cases where correlations must be taken into account, numerical simulations can be used to find solutions to Eq. (3).

Simulations

Surfaces with approximately steady-state topography were simulated using a variable time-step kinetic Monte Carlo algorithm [31,37,38]. The surfaces were initiated with the steady-state distribution of step heights calculated assuming no correlations between neighboring steps [18]. All surfaces had a length of 2^{10} (i.e., $L = 1024$), which is large enough to eliminate size effects [18]. For each set of d_N values, an ensemble of 300 statistically identical surfaces was simulated. The boundary conditions for each surface were randomly selected from within the ensemble between each reaction. The randomized boundary conditions were found to be in good agreement with the more commonly used periodic condition for large values of L and this approach more readily enables calculation of fractal dimensions. In addition, random boundary conditions allow direct comparison between simulation results and theoretical approximations based on ignoring correlations.

To ensure simulation results that were close to the steady state, each surface was subjected to 102 400 dissolution reactions. Previous work with much longer simulations initialized with flat surfaces suggested that $100 \times L$ reactions are sufficient to ensure reaction rates and surface areas that approach $\approx 99\%$ of their steady-state values [18]. Additionally, the full suite of surface topography statistics discussed below was calculated for long simulations (1×10^6 reactions) with select values of d_N. Good agreement—within one percent—was found between the long simulations and those presented below for all surface topography statistics except root-mean-square roughness and fractal roughness amplitude which showed up to 20% variability between the long and short simulations. As we discuss below, reasons for this are related to variability that is inherent to root-mean-square roughness. Variance reduction was performed using the average surface height as a control variate [39] with an expected value of zero.

III. MEASURES OF SURFACE TOPOGRAPHY

Researchers studying mineral dissolution have reported surface area, surface roughness, fractal dimension, fractal amplitude, and spacing between steps for a number of mineral-water reactions [3,40,41]. Of these five, surface area and roughness are the most commonly reported measurements. In both cases, however, there are multiple methods for obtaining measurements which lead to quite different operational definitions of the parameters (see below). The fractal dimension, fractal amplitude, and step spacing, while less frequently reported, can be calculated in an unambiguous manner from microscopic measurement of surface heights (e.g., as in atomic force microscopy, AFM) for relatively smooth surfaces [42–44]. In the following we outline some essential features of each of these measures of topography.

Surface area. Usually reported on a per mass basis known as specific surface area, this measurement is needed to interpret the rate of any surface-mediated dissolution reaction since twice the surface will usually yield twice as much product during a given amount of time. At the grain scale, two methods for measuring specific surface area are commonly employed. One—which we will refer to as BET surface area, A_{BET}—involves measuring the amount of a gas adsorbed to the surface as a function of pressure and evaluating surface area from these data using the Brunauer, Emmet, and Teller (BET) isotherm [45]. The other—which we will refer to as geometric surface area, A_{geo}—involves measuring the particle size distribution (e.g., with a series of sieves) and evaluating surface area based on the geometry of the particles [46]. It is also possible to evaluate A_{geo} by integration of height data measured microscopically on relatively flat surfaces [47], though this approach is less common.

These various ways of measuring surface area point to the fact that surface area is defined by the characteristic length scale of the "ruler" used in making the measurement [48]. In the case of BET surface area, the length scale is the size of the gas molecule being adsorbed. In fact, the BET surface area depends on the particular gas used. For geometric surface area, the size of the ruler is determined by the method used to separate particles of different sizes or to make microscopic measurements of step heights.

Surface roughness. Two surfaces with identical values of A_{geo} can have very different values of A_{BET} due to differences in the roughness of the two surfaces. As with surface area, there are two common operational definitions of surface roughness. One, which we refer to as the geometric roughness, is defined as the ratio of BET surface area to geometric surface area [49]:

$$\lambda_{\mathrm{geo}} = \frac{A_{\mathrm{BET}}}{A_{\mathrm{geo}}}. \quad (5)$$

For a perfectly smooth surface, the geometric roughness is one. There is no upper limit on λ_{geo}, though values for

naturally weathered mineral samples typically range between 10 and 1000 [16].

The other common definition of roughness, which we refer to as the root-mean-square roughness, is defined as the standard deviation of the height of the surface:

$$\lambda_{\text{rms}} = \langle (h - \bar{h})^2 \rangle^{1/2}, \tag{6}$$

where h denotes the height of the surface above some datum and the average (denoted by angle brackets) is taken over some lateral extent, L [50]. λ_{rms} and λ_{geo} are not mathematically equivalent. λ_{geo} is dimensionless, while λ_{rms} has dimensions of height. λ_{geo} is one for a perfectly smooth surface, while λ_{rms} is zero (i.e., when the datum is the height of the surface itself) and, as we discuss below, the two roughness values can vary independently of one another.

Operationally, these two types of roughness are usually measured on two distinct classes of surface. Specifically, λ_{rms} can be measured using a microscope such as an AFM to probe relatively smooth surfaces such as partially dissolved planchets [3,51–53]. In contrast, such a measurement cannot typically be performed on powders. For powders, λ_{geo} is therefore generally measured [40]. As a consequence, λ_{rms} is often used in materials science [54], but λ_{geo} is used for geochemical observations of naturally dissolved minerals [16].

Fractal dimension. One important way in which λ_{rms} and λ_{geo} differ from each other is in their dependence on the lateral extent, L, of the measurement. The definition of λ_{rms} given in Eq. (6) requires that L be specified, but the definition of λ_{geo} makes no reference to L; λ_{rms} is a function of the lateral extent and tends to increase with L, but λ_{geo} is independent of L. For self-affine surfaces, the relationship between λ_{rms} and L takes the form of a power law,

$$\lambda_{\text{rms}} \sim L^{\alpha}, \tag{7}$$

where α is the roughness index [54,55]. This index is also known as the Hausdorff measure [56] and is related to the fractal dimension by

$$\alpha = N - D, \tag{8}$$

where D is the fractal dimension and N is the dimension of the space in which the surface is embedded [57]. For surfaces of real three-dimensional objects such as minerals, $N = 3$. For our two-dimensional model system, $N = 2$.

The fractal dimension for self-affine surfaces is also related to the power spectral density, $S(f)$, for the surface,

$$S(f) \sim f^{-\beta}, \tag{9}$$

where f is the frequency and $\beta = 2\alpha + 1$ [56]. The power spectral density is the square of the magnitude of the Fourier transform of the surface height (above some datum) as a function of lateral distance. For a surface embedded in 2D,

$$S(f) = \lim_{L \to 0} \frac{1}{L} |H(f,L)|^2, \tag{10}$$

where $H(f, L)$ is the Fourier transform.

Several methods have been used to calculate fractal dimension for real surfaces. For example, in the two-dimensional fast Fourier method [54], the log power is plotted against log frequency for scans of a surface measured over different areas and at different resolutions using a microscope. This method has been used, for example, to estimate the fractal dimensions of dissolving glass and crystals of albite feldspar composition [48,53].

Values of the fractal dimension of polished or etched crystal and glass of feldspar composition have been calculated using these methods to generally range between 2.7 and 3 [53]. Likewise, the fractal dimension of optical glasses has been measured using power spectra to equal 2.65 [54]. The fractal dimension of a silicon substrate has also been observed to equal 2.74, whereas the dimension of a polysilicon layer deposited on top of the substrate by chemical vapor deposition yielded a value near 2.2 [58].

Fractal dimensions have also been estimated by comparisons of specific surface area as a function of particle size for many geological materials [41,53]. Based on this method, values of quartz and calcite are generally close to 2.0, whereas samples of dolomite, skeletal carbonates, and feldspar were reported to vary between 2.3 and 3.0 [41]. Adsorption measurements have also been used to estimate fractal dimensions of soils (2.1–2.7), apatite (2.7), bentonite (2.1–2.3), kaolinite and montmorillonite (2–2.4) [59]. Those same authors report values based on small-angle scattering that vary between 1.6 and 2.91 for soils, humic materials, clays, and sands, though the physical interpretation of values below two remains unclear.

Recently, surface fractal dimensions have been measured for unweathered crystalline rocks by performing neutron scattering on thin sections of rock. The fractal dimensions measured by this technique are applicable to nanometer-scale surface features and values obtained include 2.7 to 2.8 for basaltic andesite [60], 2.5 for quartz diorite [60], 2.6 for diabase [61], and 2.6 for granite [61].

Fractal amplitude. Equations (7) and (9), which define the fractal dimension, both implicitly include a scaling prefactor. While the fractal dimension defined by these equations is the same [56], the scaling prefactors are different. Both are, however, commonly referred to as amplitudes [57]. We denote the fractal roughness amplitude defined by Eq. (7) as a and the power spectral amplitude defined by Eq. (9) as a', so that Eqs. (7) and (9) can be written, respectively, as

$$\lambda_{\text{rms}} = a L^{N-D}, \tag{11}$$

$$S(f) = a' f^{2D-2N-1}, \tag{12}$$

where the exponents have been written in terms of the fractal dimension, D, and the embedding dimension, N (3 for real surfaces, 2 for our model system). The dimensions of a vary with D such that the left-hand side of Eq. (11) has dimensions of length. The dimensions of a' are length squared regardless of the value of D.

Step spacing. The average horizontal spacing between steps on a surface has not been broadly reported for minerals (see, however, [3,52]).This measure of surface topography can be readily evaluated from the same type of data needed for measuring λ_{rms} or the fractal dimension. Since mineral surface reactivity is likely to be heavily influenced by the density of steps, step spacing may provide a convenient way of relating surface reactivity to surface topography and so we include this

measure in our analyses on the basis of its potential value. For the 2D step model, the expected value of the step spacing, $E[s]$, is given by

$$E[s] = \frac{1}{1 - P(n = 0)}, \tag{13}$$

where $P(n = 0)$ is the probability of finding a step height of zero at a randomly selected location on the surface.

IV. MEASURES OF SURFACE TOPOGRAPHY IN THE 2D STEP MODEL

Each of the measures of surface topography defined above can be calculated for the 2D step model. Doing so allows us to see how these measures are related to one another and also how they are influenced by the chemical reactions that form and modify the surface—i.e., the values of d_1, d_2, and d_3 in Eqs. (1)–(4).

Surface area. As described above, two distinct operational definitions of surface area are in common use. The BET surface area, A_{BET}, is a measure of the total surface area at the molecular scale. For the 2D step model, A_{BET} can be calculated as the total length of the surface including the vertical line segments due to steps and the horizontal line segment between steps,

$$A_{\mathrm{BET}} = L + \sum_{i=1}^{M-1} |n_i|, \tag{14}$$

where L is the width of the surface, M is the (integer) number of crystal units in L, and the $|n_i|$ are the absolute values of the step heights. In our model, L and M are numerically equivalent, but L has dimensions of length while M is dimensionless. More generally, the ratio L/M is the crystallographic spacing.

The stochastic nature of the surface during reaction can be incorporated into Eq. (14) to give

$$A_{\mathrm{BET}} = L\left(1 + 2\sum_{n=1}^{\infty} nP(n)\right), \tag{15}$$

where the summation is now over all possible step heights and the fact that $P(n)$ is an even function is employed to give the factor of 2. Equation (15) is valid for both correlated and uncorrelated surfaces.

For uncorrelated surfaces, Eq. (4) can be substituted into Eq. (15) for $P(n)$. Provided that $d_1 > d_3$ (i.e., removal of atoms at the surface that are protruding is easier than removing an atom from a perfect surface by opening a pit) the resulting sum converges and the expression for A_{BET} is

$$A_{\mathrm{BET}} = L\left(1 + 2\frac{\sqrt{d_1/d_3}}{(\sqrt{d_1/d_3} + 1)(\sqrt{d_1/d_3} - 1)}\right). \tag{16}$$

Equation (16) has no dependence on d_2 indicating that, for an uncorrelated surface, the BET surface area depends only on the lateral extent of the surface, L, and the ratio of the step removal rate, d_1, to the step creation rate, d_3. The model parameter d_2 represents the rate at which a given step moves across the surface (step retreat). When the step locations are assumed to be uncorrelated, step retreat has no influence on the steady-state specific area of the surface.

In contrast to A_{BET}, the geometric surface area, A_{geo}, is simply equal to the width of the simulation,

$$A_{\mathrm{geo}} = L. \tag{17}$$

For the simulations considered below, $L = 2^{10}$.

Roughness. As with surface area, two definitions of roughness are commonly used. The geometric roughness is the ratio of the BET surface area to the geometric surface area. Inserting Eqs. (15) and (17) into this definition gives

$$\lambda_{\mathrm{geo}} = 1 + 2\sum_{n=1}^{\infty} nP(n). \tag{18}$$

Equation (18) can be interpreted as one plus the expected value of the step heights. Geometric roughness does not depend on the lateral extent of the surface (i.e., λ_{geo} is independent of L). This relationship holds for both correlated and uncorrelated surfaces.

Dividing Eq. (16) by L gives the following expression for the geometric roughness of an uncorrelated surface:

$$\lambda_{\mathrm{geo}} = 1 + 2\frac{\sqrt{d_1/d_3}}{(\sqrt{d_1/d_3} + 1)(\sqrt{d_1/d_3} - 1)}. \tag{19}$$

Like A_{BET}, λ_{geo} is independent of d_2/d_3 for uncorrelated surfaces. Equation (19) indicates that λ_{geo} becomes infinitely large as d_1/d_3 approaches one, and that λ_{geo} approaches one as d_1/d_3 becomes large.

The root-mean-square roughness is defined as the square root of the variance of the height of the surface [see Eq. (6)]. This definition requires the specification of a lateral extent of the surface over which the variance is to be computed. To evaluate λ_{rms} in terms of the step heights, n, consider a surface of lateral extent L whose height at location zero is denoted as h_0. All subsequent heights can then be expressed in terms of a sequence of step heights,

$$h_j = h_0 + \sum_{k=1}^{j} n_k. \tag{20}$$

The average height of the surface is then given by

$$\langle h\rangle = \frac{h_0 + (h_0 + n_1) + \cdots + (h_0 + n_1 \cdots + n_{M-1})}{M} = \frac{Mh_0 + \sum_{j=1}^{M-1} n_j(M - j)}{M}, \tag{21}$$

where M is the number of crystallographic units in a surface of extent, L. The raw second-order moment of h over the surface can be found in a similar manner:

$$\langle h^2\rangle = \frac{{h_0}^2 + (h_0 + n_1)^2 + \cdots + (h_0 + n_1 \cdots + n_{M-1})^2}{M} = \frac{{h_0}^2 M + \sum_{j=1}^{M-1} n_j\left[(n_j + 2h_0)(M - j) + \sum_{k=j+1}^{M-1} n_k(M - k)\right]}{M}. \tag{22}$$

The variance of the surface heights is the difference between Eq. (22) and the square of Eq. (21):

$$\langle h^2\rangle - \langle h\rangle^2 = \frac{1}{M}\sum_{j=1}^{M-1} {n_j}^2(M-j) - \frac{1}{M^2}\sum_{j=1}^{M-1} {n_j}^2(M-j)^2 + \frac{2}{M}\sum_{j=1}^{M-1} n_j \sum_{k=j+1}^{M-1} n_k(M-k) - \frac{1}{M^2}\sum_{j=1}^{M-1} n_j(M-j)\sum_{k=j+1}^{M-1} n_k(M-k). \tag{23}$$

Taking the average of Eq. (23) over an ensemble of surfaces gives

$$\lambda_{\text{rms}} = \sqrt{\frac{E[n^2]}{6}\left(M-\frac{1}{M}\right) + \sum_{k=1}^{M-2}\sigma_k\left(-\frac{M}{6}+\frac{1}{2}+\frac{3k^2-3k-2}{M}+\frac{-k^3+k}{3M^2}\right)}, \tag{24}$$

where σ_k is the covariance of step heights removed by a distance k,

$$\sigma_k = E[n_i n_{i+k}]. \tag{25}$$

Equation (24) indicates that λ_{rms} depends on the second-order moments—$E[n^2]$ and σ_k—of the step heights, both of which have dimensions of length squared. This is in contrast to λ_{geo} as given by Eq. (18) which depends on the first order moment of the absolute step heights—$E[|n|]$. As a result, λ_{rms} can be expected to be more sensitive to noisy data than λ_{geo} and, therefore, λ_{rms} may be more difficult to compute accurately.

Since M is numerically equivalent to the scale, L, over which the measurement is made, Eq. (24) indicates a dependence of λ_{rms} on L similar to that of Eq. (11). For an uncorrelated surface, the covariance terms are zero so Eq. (24) simplifies to

$$\lambda_{\text{rms}} = \sqrt{\frac{1}{6}E[n^2]\left(M-\frac{1}{M}\right)}. \tag{26}$$

For large M, the $1/M$ term is negligible (e.g., for the simulations considered below, $M \approx 10^3$ and $1/M \approx 10^{-3}$), so λ_{rms} is proportional to $M^{0.5}$. For the purposes of this paper, we consider $M \geqslant 2^4 (= 16)$ to be sufficiently large for the $1/M$ term in Eq. (26) to be negligible. The $E[n^2]$ in Eq. (26) can be evaluated for an uncorrelated steady-state surface using Eq. (4) and employing the even character of $P(n)$:

$$E[n^2] = \sum_{n=-\infty}^{\infty} n^2 P(n) = 2\sum_{n=1}^{\infty} n^2 \frac{\sqrt{d_1/d_3}-1}{\sqrt{d_1/d_3}+1}\left(\sqrt{d_1/d_3}\right)^{-|n|}. \tag{27}$$

The series in Eq. (27) converges when $d_1 > d_3$ giving

$$E[n^2] = \frac{2\sqrt{d_1/d_3}}{\left(\sqrt{d_1/d_3}-1\right)^2}. \tag{28}$$

The expression for λ_{rms} for an uncorrelated surface with large L becomes

$$\lambda_{\text{rms}} = \frac{\sqrt{3}}{3}\frac{\sqrt[4]{d_1/d_3}}{\sqrt{d_1/d_3}-1}\frac{1}{\sqrt{\Delta L}}L^{0.5}, \tag{29}$$

where ΔL represents the crystal spacing (equal to one in our model). As with Eq. (19) for λ_{geo}, Eq. (29) shows that uncorrelated λ_{rms} is independent of d_2/d_3, grows infinitely large as d_1/d_3 approaches one, and approaches zero (the value for a smooth surface) for large d_1/d_3. Note also from Eq. (29) that interpreting λ_{rms} always requires the specification of a length scale.

Fractal dimension. The scaling relationship between λ_{rms} and $L^{1/2}$ in Eq. (29) implies that the fractal dimension, D, of an uncorrelated surface is 1.5 [see Eq. (8) with $\alpha = 0.5$ and $N = 2$]. A 1D Brownian walk also has a fractal dimension of 1.5 [56] and a similar result has been obtained for natural and artificial random surfaces [62]. In all of these cases, the fractal dimension of 1.5 is a result of the uncorrelated nature of the steps on the surface.

It is not true, however, that $D = 1.5$ uniquely implies an uncorrelated surface. Equation (24), which is applicable to both correlated and uncorrelated surfaces, yields a fractal dimension of 1.5 for a broad range of cases. One such case is when σ_k is constant up to some maximum value of k and zero thereafter, provided that the following condition is met:

$$\sigma_k < \frac{E[n^2]}{k_{\text{cutoff}}}, \tag{30}$$

where k_{cutoff} is the distance above which the covariance is zero. For surfaces satisfying Eq. (30), the summation in Eq. (24) is dominated by the leading $-M/6$ term such that λ_{rms} scales with $L^{1/2}$ for large L.

The fractal dimension is also 1.5 when σ_k is proportional to f^k with $0 < f < 1$, again provided that the short-range covariances are not too large. The condition for $D = 1.5$ in this case can be written as

$$\sum_{k=1}^{\infty}\sigma_k < E[n^2]. \tag{31}$$

As in the case with the cutoff covariances, here the fractal dimension is 1.5 because a leading term that is proportional to L dominates the summation in Eq. (24). This discussion leads to the conclusion that a fractal dimension of 1.5 generally arises when the long-range correlations between steps die off rapidly enough and when the short-range correlations are sufficiently small. Again, likening these attributes to known attributes of crystal surfaces, these criteria might be met when a real crystal has randomly distributed defects. In this case, spacing of steps is likely to show small short-range correlations and long-range correlations that die off rapidly. Given this observation, surfaces of glasses might be expected to approach

fractal dimensions of 2.5 (where fractal dimensions for our 2D model system can be compared to 3D solids by adding one [56], though fractal properties of surfaces can change dramatically when moving from 2D to 3D spaces).

Fractal dimensions other than 1.5 can be found for cases with large short-range correlations. For example, if σ_k is constant for $k < k_{\text{cutoff}}$ and zero thereafter, then $D = 2$, provided that

$$\sum_{k=1}^{\infty} \sigma_k = E[n^2]. \tag{32}$$

A fractal dimension of 2 also arises from Eq. (24) when $\sigma_k \sim f^k$ when the constant of proportionality is selected such that Eq. (32) is met. In both of these cases, the leading M term in the summation of Eq. (24) exactly balances the $E[n^2] \cdot M/6$ term so that the remaining expression is independent of L for sufficiently large L.

Figure 2 shows two ensembles of surfaces generated with the 2D step model described above. The surfaces in Fig. 2(a) have an average fractal dimension of 1.5, while the surfaces in Fig. 2(b) have an average fractal dimension of 1.99. Both of these ensembles have approximately the same $\lambda_{\text{rms}}(\approx 7)$ at the length scale $L = 1024$. This can be seen in Fig. 2 by noting that both ensembles have the same spread of heights at $L = 1024$. The two ensembles are, however, very different in the rate at which the heights spread out as the length increases from 0 to 1024. It is this difference in rate of spread that is described by the fractal dimension, D.

The surfaces in Fig. 2(a) spread out gradually, like a square root function (similar to a Brownian walk). The surfaces in Fig. 2(b) spread out immediately—before $L = 50$—and the spread increases only a little thereafter. These differences are characterized by the fractal dimension according to Eq. (7). The surfaces in Fig. 2(a) have an average D of 1.5 (as calculated from the power spectra) and this is precisely because of the square-root-like spread of the surfaces. The surfaces in Fig. 2(b) have an average D of 1.99 due to the nearly zero rate of long-term spreading in the surfaces.

The fractal dimensions of the surfaces in Fig. 2 are consistent with the above discussion of covariance. The highlighted surface with lower fractal dimension in Fig. 2(a) has a smooth appearance when compared to the highlighted surface with higher D in Fig. 2(b). This is because the steps that comprise the surface in Fig. 2(a) are uncorrelated, while the steps that comprise the surface in Fig. 2(b) have strong positive short-range correlations that die off to zero with increasing distance. The correlation between steps in Fig. 2(b) is evident in the spiky nature of the surface—any positive (negative) step is likely to be followed by several more positive (negative) steps. When considered in the embedding dimension of 3, such a surface with high fractal dimension is often described as "space filling."

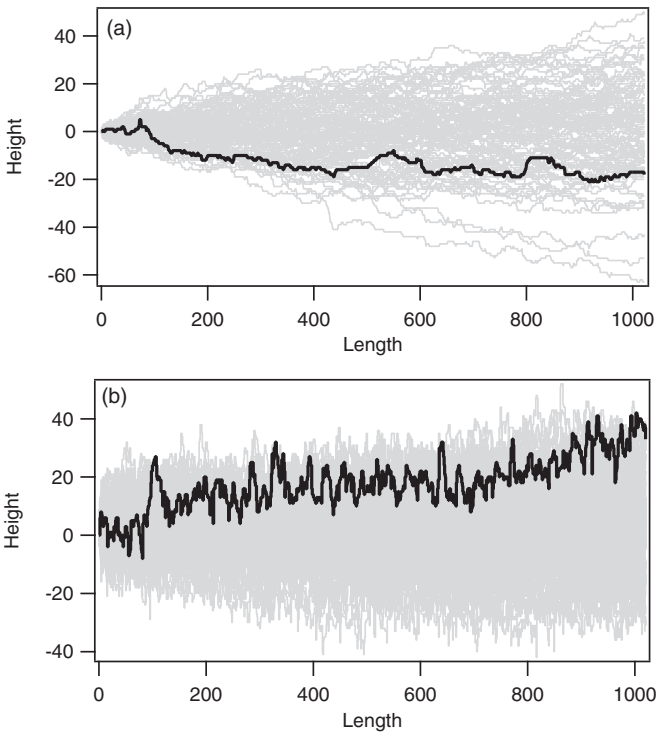

FIG. 2. Ensembles of surfaces generated with the 2D step model for (a) $d_1/d_3 = 128$ and $d_2/d_3 = 64$ and (b) $d_1/d_3 = 1024$ and $d_2/d_3 = 1$. For both cases, one particular surface is highlighted in black. Both ensembles have an average $\lambda_{\text{rms}} \approx 7$ but (a) has $D = 1.5$ while (b) has $D = 1.99$.

Equation (24) also permits values of the fractal dimension that are less than 1.5. For example, substituting a constant positive covariance with no maximum cutoff into Eq. (24) gives

$$\lambda_{\text{rms}} = \sqrt{\frac{1}{6}E[n^2]\left(M - \frac{1}{M}\right) + \sigma\left(\frac{3}{4}M^2 - \frac{14}{3}M + \frac{31}{12} - \frac{3}{2M}\right)}, \tag{33}$$

where σ denotes the constant positive covariance. For large values of M, Eq. (33) is dominated by the M^2 term such that λ_{rms} is proportional to L^1 and, therefore, $D = 1$. In our simulations with the 2D step model, however, we have not observed a fractal dimension less than 1.5, even though we performed simulations over a very wide swath of the d_1/d_3, d_2/d_3 space (see Fig. 4).

Taken together, these results indicate that (i) fractal dimensions less than 1.5 are associated with long-range correlations; (ii) fractal dimensions equal to 1.5 are associated with surfaces with, at most, weak correlations between steps, and (iii) fractal dimensions greater than 1.5 are associated with surfaces with strong short-range correlations. In this regard, it is noteworthy that Farin and Avnir (1987) report that

crystals of calcite (Iceland spar) or quartz that are relatively defect free are characterized by values of $D = 1.8-2.45$ and 2.0, respectively, while crystals of the chemically complex minerals dolomite and feldspar which are always more defect laden are typically reported to have higher values of D. Crystals which contain defects that are widely spaced are likely to show long-range order ($D < 2.5$), while crystals with closely spaced defects are likely to only show short-range order ($D > 2.5$).

Fractal amplitude. The fractal roughness amplitude, a, defined by Eq. (11) is a function of the second-order moments, $E[n^2]$ and σ_k. For the uncorrelated case, Eq. (29) can be used to identify a as

$$a = \frac{\sqrt{3}}{3} \frac{\sqrt[4]{d_1/d_3}}{\sqrt{d_1/d_3} - 1} \frac{1}{\sqrt{\Delta L}}. \tag{34}$$

Equation (34) indicates that, for uncorrelated surfaces, a depends only on d_1/d_3. Therefore, any dependence on d_2/d_3 implies correlation between the steps.

The fractal roughness amplitude can be related to the power spectrum amplitude [a' in Eq. (12)] using Parseval's theorem [57]. For a surface embedded in 2D, the resulting relation is

$$a' = \frac{a^2 \Delta L^{4-2D}}{(2\pi)^{2D-5} \sum_{p=1}^{M-1} p^{(2D-5)}}. \tag{35}$$

Note that for a surface embedded in 3D, the powers in the denominator of Eq. (35) must be modified; see Ref. [57] for details. Equation (35) implies that the two fractal amplitudes are never independent measures of surface topography since one of them can always be calculated from the other.

For an uncorrelated surface, $D = 1.5$, and a is given by Eq. (34). Substituting these into Eq. (35) gives

$$a' = \frac{\sqrt{d_1/d_3}\Delta L}{3(\sqrt{d_1/d_3} - 1)^2 (2\pi)^{-2} \sum_{p=1}^{M-1} p^{-2}} \approx \frac{8\sqrt{d_1/d_3}\Delta L}{(\sqrt{d_1/d_3} - 1)^2}, \tag{36}$$

where the approximation holds for large L since the series $1 + 1/4 + 1/9 + 1/16 + \cdots = \pi^2/6$. As with the other measures of surface topography, a' is independent of d_2/d_3 for uncorrelated surfaces.

Step spacing. Substituting Eq. (4) with $n = 0$ into Eq. (13) yields the following expression for average step spacing on an uncorrelated surface:

$$E[s] = \frac{\sqrt{d_1/d_3} + 1}{2}. \tag{37}$$

The step spacing for an uncorrelated surface is independent of d_2/d_3, approaches one as d_1/d_3 approaches one, and approaches ∞ for large d_1/d_3. A step spacing of 1 corresponds to a rough surface with a nonzero step at every surface site, while large values of $E[s]$ correspond to smooth surfaces.

V. SIMULATION RESULTS

Geometric roughness. Figure 3(a) shows contours of constant λ_{geo} for our simulations plotted in the space of d_1/d_3 vs d_2/d_3. Mathematically, d_1/d_3 and d_2/d_3 must always be > 0. However, since d_3 represents the formation of a step in a flat surface, d_2 represents the retreat of steps, and d_1 represents the ultimate removal of a stepped layer, it is physically realistic to further expect that $d_1 \geqslant d_2 \geqslant d_3$. Therefore, we have focused our simulations on values of d_1/d_3 and d_2/d_3 greater than one. [Note also that the region where $d_1 \geqslant d_2$ is the upper left half of Fig. 3(a).]

The geometric roughness approaches one as both d_1/d_3 and d_2/d_3 become large [the upper right corner of Fig. 2(a)]. This occurs—for example, during so-called chemical polishing—because the rates of step retreat (d_2) and disappearance (d_1) are much greater than the rate at which steps are formed (d_3) so that the steady-state surface has very few steps. Decreasing either d_1/d_3 or d_2/d_3 leads to an increase in λ_{geo}, though the change is more rapid as a function of variation in d_1/d_3. When d_1/d_3 is close to one and d_2/d_3 is large [the lower right corner of Fig. 3(a)], the steady-state surface is dominated by sites

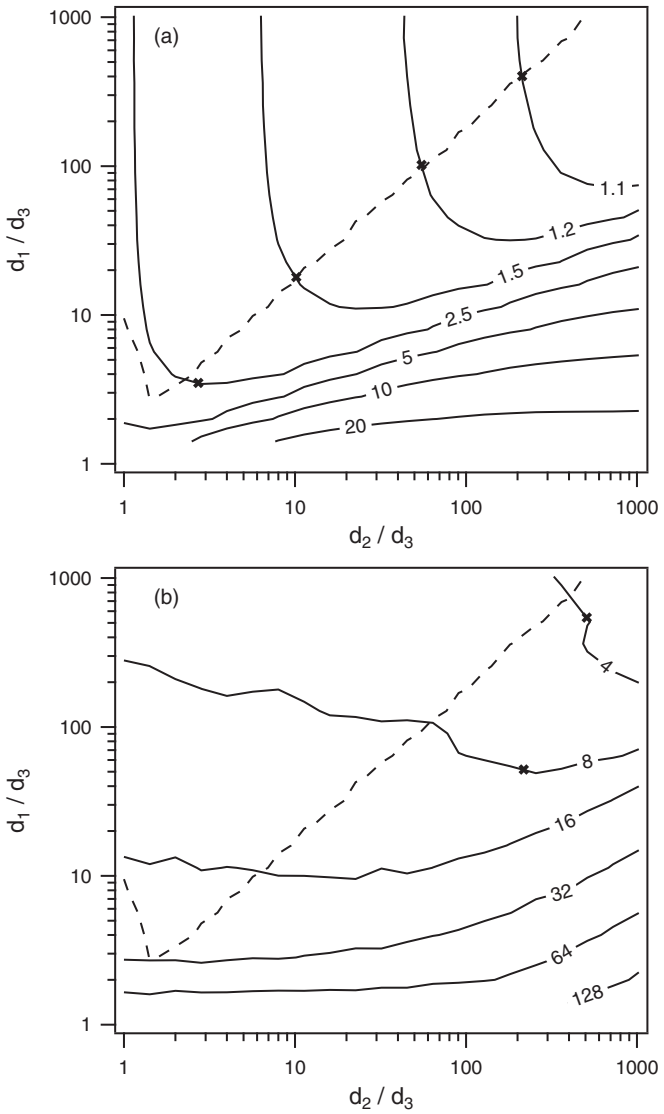

FIG. 3. Solid lines represent contours of constant (a) geometric roughness and (b) root-mean-square roughness plotted in the space of d_1/d_3 vs d_2/d_3. Dashed line represents the contour where $\sigma_1 = 0$ and markers represent locations where simulated roughness contours intersect uncorrelated approximations given by Eqs. (19) and (29).

with either one or three nearest neighbors because any steps that form quickly retreat. The resulting surface is comprised of large towers of one unit width and has a correspondingly large value of λ_{geo}. When d_1/d_3 equals one, a steady-state surface was not reached in our simulations and, at least in the case of $d_1 = d_2 = d_3$, no steady state exists because all surface sites dissolve with equal probability.

When d_2/d_3 is close to one and d_1/d_3 is large [upper left of Fig. 3(a)], the rates of step formation and retreat are equal and the ultimate removal of steps is nearly instantaneous so that the surface is comprised of roughly equal numbers of steps and flat surface. The resulting surface has a moderate value of $\lambda_{geo} \approx 2.5$. The λ_{geo} values in our simulations can be compared to measured values for real surfaces by squaring our simulation results (this is due to the difference in dimensionality). For example, the observed values of λ_{geo} typically range from 10 to 1000 for natural samples [16]. The square of our simulated values ranges from nearly 1 to 820. Simulated values where $d_1 \geqslant d_2 \geqslant d_3$, however, did not exceed 46 [this value is obtained in the lower left region of Fig. 3(a)]. The poor agreement can be attributed to the fact that the Ising model used here does not incorporate overhangs and that the very high roughness of some natural samples has been attributed to porosity [53].

The "x" symbols in Fig. 3(a) represent the location on each contour where the uncorrelated approximation of λ_{geo} given by Eq. (19) is the same as the simulation results. Note that since Eq. (19) depends only on d_1/d_3, contours of constant of λ_{geo} calculated from Eq. (19) would appear as horizontal lines in Fig. 3(a). The markers represent the intersection of these horizontal lines with the contours generated from the simulation results.

The dashed line in Fig. 3(a) represents the contour where $\sigma_1 = 0$. Higher-order covariances are also zero along this contour, except where d_2/d_3 begins to approach 1 [i.e., on the left side of Fig. 3(a) where the $\sigma_1 = 0$ contour forms an upward "hook"]. The intersections of Eq. (19) and the simulation results all fall near the $\sigma_1 = 0$ contour (within 15%). This indicates that the uncorrelated model represented by Eq. (4) is correct along the $\sigma_1 = 0$ contour provided that d_2/d_3 is not too small. (For values of $d_2/d_3 > 2.5$, none of the higher-order covariances has a magnitude greater than 0.1 for our simulations.)

Since the $\sigma_1 = 0$ contour appears to be a straight line in the log-scaled space of Fig. 3(a), the region in d_1/d_3 vs d_2/d_3 space where steps are uncorrelated can be represented by a power law:

$$\frac{d_1}{d_3} = 1.31\left(\frac{d_2}{d_3}\right)^{1.07}, \tag{38}$$

where we have assumed the condition $d_2/d_3 > 2.5$ as described above. In the vicinity of Eq. (38), we can expect a fractal dimension of 1.5 per Eq. (29) and this is borne out by Fig. 4. Moreover, in the vicinity of Eq. (38), all surface topography statistics are uniquely determined by d_1/d_3. Therefore, only the ratio of the step removal rate (d_1) to the step creation rate (d_3) can be determined from any measure of surface topography.

Root-mean-square roughness. Figure 3(b) shows contours of constant λ_{rms} for the same simulations discussed above. Like

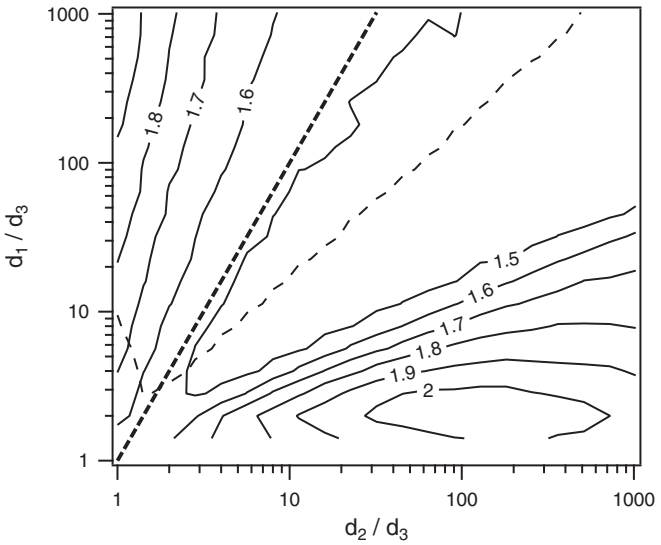

FIG. 4. Solid lines represent contours of constant fractal dimension plotted in the space of d_1/d_3 vs d_2/d_3. The light dashed line represents the contour where $\sigma_1 = 0$. The thick dashed line represents an exponential relationship between the d_i.

λ_{geo}, root-mean-square roughness decreases as both d_1/d_3 and d_2/d_3 increase. However, the shape of the contours is quite different, indicating that λ_{geo} and λ_{rms} vary independently of one another. Plotting these two variables against each other (not shown) confirms this. The independence of λ_{geo} and λ_{rms} suggests that simultaneous measurements of these parameters describing surface topography could be used to determine d_1/d_3 and d_2/d_3, provided that sufficiently strong correlations are present [i.e., provided that the region around the dashed line in Fig. 3(a) is avoided]. For instance, for our steady-state model surfaces, if $\lambda_{geo} = 1.75$ and $\lambda_{rms} = 50$, then reading from Fig. 3, the ratios d_1/d_3 and d_2/d_3 would have values of approximately 25 and 4, respectively.

Unfortunately, there are at least two difficulties with this approach. First, as described earlier, both roughness statistics are generally not measured for the same surface. Root-mean-square roughness is usually measured by techniques that are limited to relatively smooth surfaces [53], while geometric roughness is usually measured by a technique (BET surface area analysis of a powder with well-characterized size distribution) that is limited to relatively rough surfaces [46].

While this first difficulty could, perhaps, be overcome by creative technique development, a second difficulty is more intractable: λ_{rms} is an inherently noisy measurement. The percent error calculated by averaging the ratio of the ensemble standard deviation divided by the ensemble average was found to be 37% for $L = 1024$ and was unchanged for successively smaller values of L down to $L = 128$. Constant percent error in λ_{rms} with respect to L was confirmed for larger values of L (up to $L = 2^{17}$) using ensembles of uncorrelated surfaces generated from Eq. (4). On average, λ_{rms} was found to have 40% error for uncorrelated surfaces when $d_1/d_3 = 8$. Taken together, these results indicate that substantial error is inherent to the measurement of λ_{rms} for fractal surfaces. The large error inherent in λ_{rms} is the reason why the intersections—represented by "x" symbols—of the

λ_{rms} contours with Eq. (34) for uncorrelated surfaces do not fall directly on the dashed line representing covariance of zero.

Fractal dimension. Figure 4 shows contours of constant D in the space of d_1/d_3 vs d_2/d_3. Fractal dimension approaches its maximum value of 2 for large values of d_1/d_3 and small values of d_2/d_3, and D decreases with either decreasing d_1/d_3 or increasing d_2/d_3. The fractal dimension is a measure of the dimensionality of the model surface with values approaching 2 characteristic of plane-filling surfaces and values approaching 1 characteristic of a Euclidian surface (e.g., a flat line). Note, however, that D is not a measure of surface roughness since by comparing Fig. 4 with Fig. 3 we see that surfaces with $D = 1.5$ can have nearly any value of roughness and D can decrease while roughness increases (compare, also, Fig. 2).

In the center region of Fig. 4, there is a wedge-shaped plateau where $D = 1.5$. This value of the fractal dimension is characteristic of surfaces where correlations between steps die off sufficiently fast with distance. The light dashed contour in Fig. 4 shows the region where the covariance between neighboring steps is approximately zero. This contour crosses the $D = 1.5$ contour when $d_1/d_3 = 4$ and $d_2/d_3 = 2.55$, which corresponds well with the region where longer-range covariances are zero.

We have not investigated the precise rate of decay of σ_k necessary to ensure $D = 1.5$; however, any surface where $\sigma_k \leqslant f^k$ ($|f| < 1$) for all k will have $D = 1.5$. The equality $\sigma_k = f^k$ is the solution to the one-dimensional Ising model at equilibrium under Glauber dynamics [63] where f is equal to the order parameter, $\tanh(J/k_BT)$, where J is the interaction energy of neighboring spins, k_B is the Boltzmann constant, and T is the absolute temperature. A form of this equation is often used to represent the energy dependence of bond-breaking reactions [64]. This correspondence suggests that the additive bond energy model for rate constants that is most commonly used when simulating the growth or dissolution of realistic crystals [32,35] may describe the boundary of the region where $D = 1.5$.

In our 2D step model, the additive bond energy approach can be written as

$$d_n = d_0 \exp\left(-\frac{n\phi}{k_B T}\right), \tag{39}$$

where the d_n are the same dissolution rate constants as given in Eq. (1), d_0 is a scaling constant, and ϕ is the bond energy. Equation (39) can be represented in the space of d_1/d_3 vs d_2/d_3 as

$$\log\left(\frac{d_1}{d_3}\right) = 2\log\left(\frac{d_2}{d_3}\right). \tag{40}$$

Equation (40) is shown in Fig. 4 as a heavy dashed line and, indeed, that line does appear to fall close to the portion of the $D = 1.5$ contour that serves as an upper bound to the region where fractal dimension is 1.5. This suggests that the additive bond energy model represented by Eq. (39) may not be appropriate when experimental observations suggest a fractal dimension that is significantly larger than 2.5 for a weathered mineral surface. For example, fractal dimensions for chemically simple and defect-free minerals (Iceland spar and Madagascar quartz) are both close to 2, whereas values for chemically complex and defect-laden crystals (feldspar and dolomite) are closer to 3 [41].

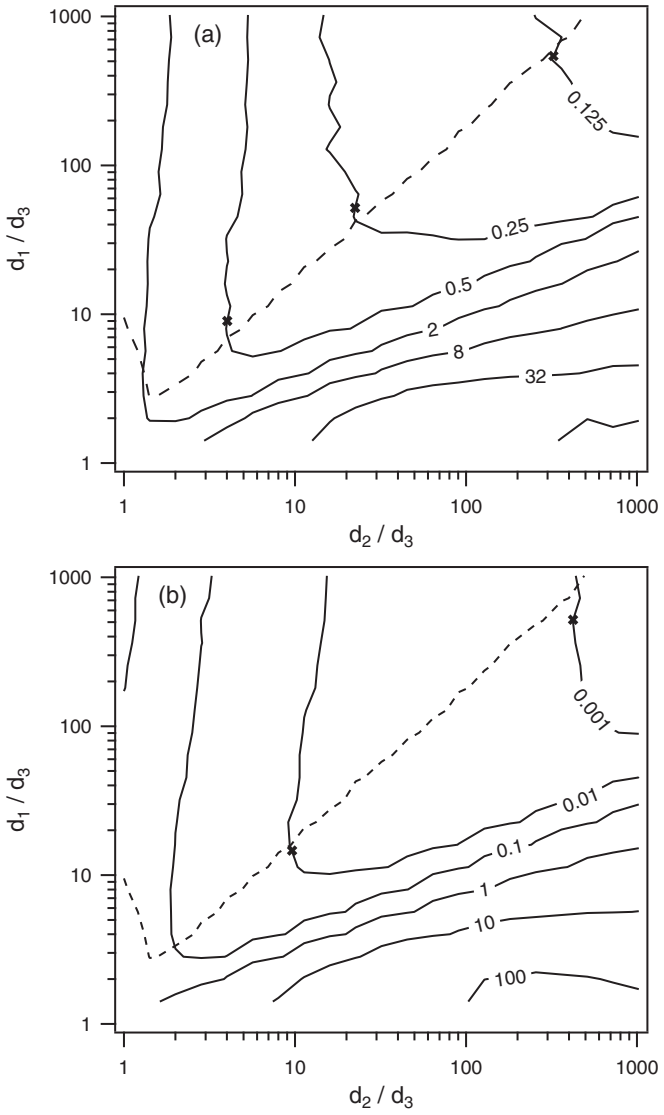

FIG. 5. Contours of constant (a) fractal roughness amplitude, a, and (b) power spectrum amplitude, a', plotted in the space of d_1/d_3 vs d_2/d_3. The dashed line represents the contour where $\sigma_1 = 0$ and markers represent locations where simulated amplitude contours intersect uncorrelated approximations given by Eqs. (34) and (36).

Fractal amplitude. Figure 5 shows contours of constant fractal roughness amplitude, a [Fig. 5(a)] and power spectrum amplitude, a' [Fig. 5(b)]. Both amplitudes decrease as d_1/d_3 and d_2/d_3 increase. Moreover, the contours of constant a and a' have essentially identical shapes, indicating a functional relationship between these variables. This observation supports the relationship given in Eq. (35); furthermore, calculating a' from Eq. (35) produces a contour plot generally identical to Fig. 5(b).

The amplitude contours shown in Fig. 5 also appear, in broad terms, to follow a shape similar to the λ_{geo} contours shown in Fig. 3(a). Both surfaces decrease as d_1/d_3 and d_2/d_3 increase, contain a valley running from the lower left to the upper right corners of the respective figures, and appear to become independent of d_1/d_3 when that variable becomes large. This last point can be seen in Figs. 2 and 5 by noting that the contours approach vertical lines for large d_1/d_3.

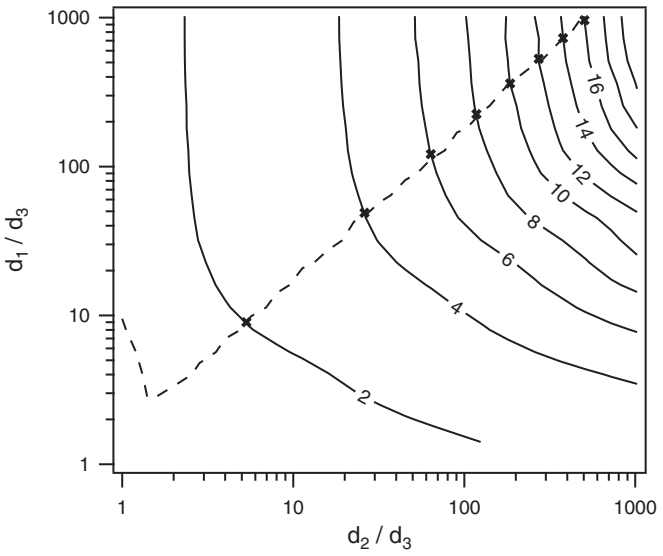

FIG. 6. Contours of constant step spacing plotted in the space of d_1/d_3 vs d_2/d_3. The dashed line represents the contour where $\sigma_1 = 0$ and markers represent locations where simulated step spacing contours intersect uncorrelated approximations given by Eq. (37).

The similarity between a and λ_{geo} indicates that the fractal roughness amplitude can be thought of as a measure of surface roughness. The same is true of the power spectrum amplitude, a', because of its relationship to a through Eq. (35). As noted above, this is not true of the fractal dimension itself which measures the spatial scaling of the roughness.

Step spacing. Figure 6 shows contours of constant step spacing, $E[s]$, for our simulations. The minimum possible value of $E[s]$ is one and when this value is approached, there are no perfectly flat $n = 0$ sites on the surface. In Fig. 6, $E[s]$ appears to approach one as d_1/d_3 and d_2/d_3 both approach one, though no simulations were performed in the case where both $d_1/d_3 = 1$ and $d_2/d_3 = 1$ because a steady-state surface does not exist under those conditions [18]. As d_1/d_3 and d_2/d_3 increase, the spacing between steps increases, resulting in the smoother surfaces already noted in Fig. 3. Since d_3 controls the rate at which steps are created and d_1 and d_2 combine to control the rate of step removal, increasing either d_1/d_3 or d_2/d_3 tends to decrease the number of steps on the surface and the step spacing increases correspondingly.

Although step spacing decreases in the same general direction through which λ_{geo}, a, and a' increase, the shape of the $E[s]$ surface is sufficiently different from those other surfaces to suggest that step spacing may represent an independent measure of surface topography. Moreover, the type of data needed to compute step spacing for real surfaces—e.g., microscopic measurement of heights over distance—is also the type of data needed to compute fractal dimension and fractal roughness amplitude. Therefore, it appears that D, a, and $E[s]$ are all good candidates for measures of surface topography that are mathematically independent of one another and that can be practicably measured for real surfaces. Once again, however, while authors often analyze step spacing during dissolution of minerals, such measurements are not generally complemented by measurements of D and a [3]. The model simulations shown here point toward the utility of such complete sets of measurements.

TABLE I. Spearman rank-order correlation coefficients for simulated topography statistics.

	λ_{geo}	λ_{rms}	D	a	a'	$E[s]$
λ_{geo}	1					
λ_{rms}	0.87	1				
D	0.81	0.51	1			
a	0.98	0.85	0.84	1		
a'	0.99	0.81	0.87	0.99	1	
$E[s]$	−0.74	−0.55	−0.50	−0.68	−0.70	1

Independence of surface topography parameters. Table I shows Spearman rank-order correlation coefficients, r_{Sp}, for each pair of surface topography measures that we considered above. Rank-order correlation is similar to the more familiar Pearson's r, but it is nonparametric and measures the extent to which two variables are monotonically related whether or not that relationship is linear. In ordinary applications of correlation analysis, one seeks values of r that are close to one. In this case, however, we are interested in those surface topography statistics that are not well correlated and therefore we are looking for values of r_{Sp} that are small. Sets of parameters that are not well correlated are measurements that should be targeted to understand surface topographies.

By this measure, D and $E[s]$ is the pair of topography measures most independent of one another with $r_{Sp} = -0.50$. By implication, measurement of these two parameters would yield the most information about the surface. Root-mean-square roughness produces relatively low values of r_{Sp} when paired with either D or $E[s]$. However, since our simulations indicate that λ_{rms} is plagued by large and intractable measurement error for fractal surfaces, we leave it out of our analysis. Ignoring λ_{rms} leaves a and $E[s]$ as the next most independent pair of topography measures with $r_{Sp} = -0.68$. Since a and a' are directly related to each other by Eq. (35), $E[s]$ and a' also form a relatively independent pair with $r_{Sp} = -0.70$. Since we anticipate power spectral data being the most convenient means of obtaining fractal dimensions for real surfaces, we will focus on D, $E[s]$, and a' as the most useful topography measures for constraining reaction mechanisms.

Figure 7 shows the three surface topography measures that we have identified as being potentially independent plotted against each other. Figure 7(a) shows a general relationship between D and a suggesting that $r_{Sp} > 0.8$ in Table I is indicative of dependence between topography measures. Plotting other pairs of variables with $r_{Sp} > 0.8$ confirms this impression (not shown).

Figures 7(b) and 7(c) partially confirm the independence of $E[s]$ with both D and a' that is indicated by the low values of r_{Sp} in Table I. Focusing on those simulations that produced a step spacing of around 10 units or less, we see a wide range of values for both D and a'. For step spacing greater than 10, however, Figs. 7(b) and 7(c) indicate a functional dependence of both D and a' on $E[s]$. This dependence can be understood by observing that the simulations fall close to the uncorrelated relationships which are displayed in Fig. 7 as

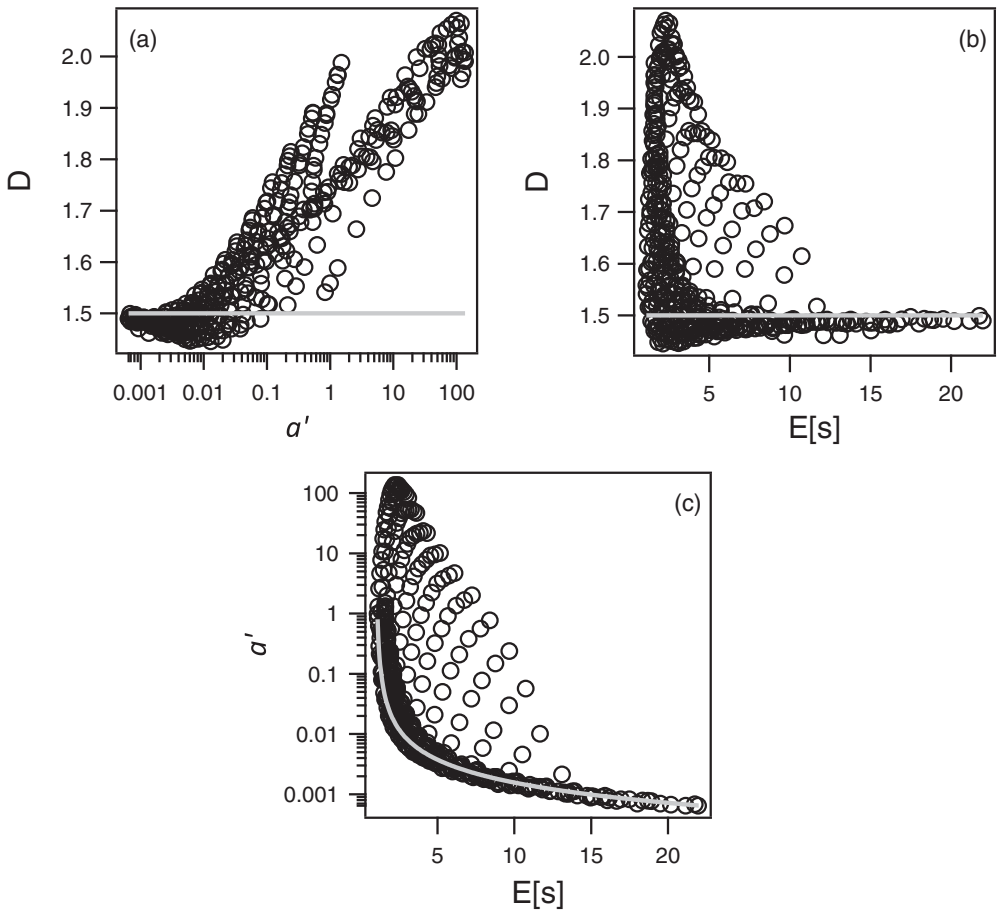

FIG. 7. Simulated fractal dimension, power spectral amplitude, and step spacing plotted against each other as open circles. Gray curves represent the uncorrelated case.

gray curves. In the case of D vs $E[s]$, the uncorrelated curve is given by $D = 1.5$. For a' vs $E[s]$, the uncorrelated curve is found by solving Eq. (37) for d_1/d_3 and substituting into Eq. (36). As discussed above, the topography of uncorrelated surfaces depends only on the value of d_1/d_3. As a result, there is only one degree of freedom in the reaction mechanism and, therefore, any measure of surface topography will contain all of the mechanistic information possible.

Constraining reaction mechanisms for the 2D step model. The independence of D, $E[s]$, and a' described above implies that d_1/d_3 and d_2/d_3 can be uniquely determined from knowledge of two of these surface topography statistics. The procedure for doing so depends, however, on the nature of the correlations between the steps. If D is greater than 1.5, then our results indicate that the steps are uncorrelated. In this case, d_1/d_3 and d_2/d_3 can be found by overlaying two topography contour plots and finding the intersection of the relevant contours. For example, the $D = 1.7$ contour in Fig. 4 intersects the $a' = 0.1$ contour in Fig. 5(b) at $d_1/d_3 = 180$ and $d_2/d_3 = 2.7$.

If D is approximately equal to 1.5, then D cannot be used as one of the independent measures of surface topography. In this case, it can still be possible to use other measures of topography such as $E[s]$ and a' and search for intersecting contours as described above. For example, the $a' = 0.01$ contour in Fig. 5(b) intersects the $E[s] = 4$ contour in Fig. 6 at $d_1/d_3 = 15$ and $d_2/d_3 = 64$. This approach is complicated, however, by the existence of a direct relationship between a' and $E[s]$ in the case of uncorrelated steps [see the gray line in Fig. 7(c)] and the fact that this relationship holds in approximate form for the bulk of cases where $D = 1.5$ because a fractal dimension of 1.5 implies relatively weak correlations. The same would hold for any other pair of topography statistics since d_1/d_3 uniquely determines the structure of the surface in the uncorrelated case.

In the case of $D = 1.5$, then, additional information is needed to fully constrain the reaction mechanism. If $D = 1.5$ and it can be assumed that the reaction mechanism obeys Eq. (39)—a common assumption in chemical kinetics—then a single measure of surface topography can be used. For example, if $E[s] = 4$, then the intersection of that contour in Fig. 6 and Eq. (40) would indicate that $d_1/d_3 = 362$ and $d_2/d_3 = 19$. On the other hand, if direct measurement of correlations between steps can be used to show that the surface is uncorrelated, Eq. (38) could be employed in a similar fashion.

VI. CONCLUSIONS

The results described above are directly applicable only to the simple 2D model depicted in Fig. 1. However, a number of the lessons can be drawn more broadly for real surfaces

by identifying those features of our model that correspond to features of real minerals. First, since the steady-state topography of both our simple model and real surfaces is determined by site-specific rate constants, measures of surface topography can determine at most the ratio of those rate constants. Therefore, just as we have sought to identify at least two independent measures of surface topography that can be used to uniquely constrain d_1/d_3 and d_2/d_3, the number of topography parameters needed for real surfaces would be one fewer than the number of site types.

Second, just as our model surface is comprised of a series of steps that possess some average spacing and, potentially, correlations in regard to their relative locations, real surfaces are comprised of steps. However, steps on real surfaces extend across the surface and move by the formation and migration of kinks. This additional structure of steps on real surfaces means that the definitions of the surface topography statistics will be more complicated and that relationships with site-specific rate constants will be difficult to determine mathematically. Nevertheless, the fractal character of real surfaces is well established and the fractal dimension for our 2D model can be compared to real surfaces by adding one to our model results. Therefore, we can conclude that fractal dimensions for real surfaces greater than 2.5 are associated with strong short-range correlations between steps—which we have argued may be applicable especially to chemically complex and defect-laden minerals—while fractal dimensions equal to 2.5 are indicative of correlations that die off quickly with distance.

Moreover, since the steps on real surfaces can be broadly characterized in terms of their rates of nucleation, retreat, and ultimate removal, and since these rates are directly analogous to our model parameters d_3, d_2, and d_1, respectively, we can conclude that step retreat rates will strongly influence surface topography only when strong correlations exist between steps. Combined with our results on fractal dimension, this means that relative retreat rates are likely to be evident in measures of surface topography only when the fractal dimension is greater than 2.5. Since, in our model, Eq. (39) appears to form a boundary for the $D = 1.5$ region, it is possible that this classical rate model where activation energy is equal to the sum of the bond energies also forms a boundary where step retreat rates cease to influence surface topography; however, further study is needed to determine if such a rate model leads to fractal dimension of 2.5 for real 2D mineral surfaces.

Lastly, in our model simulations, the fractal parameters, D and a', proved to be the most mechanistically sensitive measures of surface topography, particularly when coupled with the expected spacing between steps, $E[s]$. Since this result arises from the fractal character of our model surface and since real mineral surfaces can be expected to be fractal [41,53,62], it is likely that these same topography parameters will be useful to constrain reaction rates and to diagnose reaction mechanisms. In this regard, it is notable that λ_{rms} was found to be an inherently noisy measure of surface topography in our model simulations. This result also arises from the fractal character of our model and may limit the utility of λ_{rms} for characterizing minerals as well as other types of reactive surfaces. It is, therefore, advisable to characterize the roughness of fractal surfaces using parameters such as fractal dimension, power spectral amplitude, and step spacing rather than root-mean-square roughness.

ACKNOWLEDGMENTS

This work was funded by Grant No. DE-FG02-0SER15675 from the Department of Energy's Office of Basic Energy Sciences (S.L.B.). J.Z.B. acknowledges support by the National Science Foundation under Grant No. DUE-1161227.

[1] G. H. Gilmer, Mater. Sci. Eng. **65**, 15 (1984).
[2] K. A. Jackson, G. H. Gilmer, D. E. Temkin, and K. M. Beatty, J. Cryst. Growth **163**, 461 (1996).
[3] P. M. Dove, N. Han, and J. J. De Yoreo, Proc. Natl. Acad. Sci. USA **102**, 15357 (2005).
[4] P. Maksym, Semicond. Sci. Technol. **3**, 594 (1988).
[5] G. A. Icopini, S. L. Brantley, and P. J. Heaney, Geochim. Cosmochim. Acta **69**, 293 (2005).
[6] W. W. Barker and J. F. Banfield, Geomicrobiology J. **15**, 223 (1998).
[7] I. Chang, E. S. Gilbert, N. Eliashberg, and J. D. Keasling, Microbiology **149**, 2859 (2003).
[8] S. M. Hunt, M. A. Hamilton, J. T. Sears, G. Harkin, and J. Reno, Microbiology **149**, 1155 (2003).
[9] M. G. Fernandes, R. M. Latanision, and P. C. Searson, Phys. Rev. B **47**, 11749 (1993).
[10] Y. Liang and D. R. Baer, Surf. Sci. **373**, 275 (1997).
[11] L. Jin, R. Ravella, B. Ketchum, P. R. Bierman, P. Heaney, T. White, and S. L. Brantley, Geochim. Cosmochim. Acta **74**, 3669 (2010).
[12] A. C. Lasaga and A. Luttge, Am. Mineral. **89**, 527 (2004).
[13] A. C. Lasaga and A. Luttge, Science **291**, 2400 (2001).
[14] A. Luttge, E. W. Bolton, and A. C. Lasaga, Amer. J. Sci. **299**, 652 (1999).
[15] S. L. Brantley, A. Blai, I. MacInnis, D. Cremeens, and D. Darmody, Aquatic Sci. **55**, 262 (1993).
[16] A. F. White and S. L. Brantley, Chem. Geol. **202**, 479 (2003).
[17] A. F. White, in *Kinetics of Water-Rock Interaction*, edited by S. L. Brantley, J. D. Kubicki, and A. F. White (Springer, New York, 2008), p. 469.
[18] J. Z. Bandstra and S. L. Brantley, Geochim. Cosmochim. Acta **72**, 2587 (2008).
[19] W. K. Burton, N. Cabrera, and F. C. Frank, Philos. Trans. R. Soc. London **243**, 299 (1951).
[20] H. M. Cuppen, H. Meekes, W. J. P. van Enckevort, P. Bennema, and E. Vlieg, Surf. Sci. **525**, 1 (2003).
[21] H. M. Cuppen, H. Meekes, E. van Veenendaal, W. J. P. van Enckevort, P. Bennema, M. F. Reedijk, J. Arsic, and E. Vlieg, Surf. Sci. **506**, 183 (2002).
[22] D. E. Temkin, Sov. Phys. Crystallogr. **14**, 179 (1969).
[23] J. M. Deutch and P. Meakin, J. Chem. Phys. **78**, 2093 (1983).

[24] G. H. Gilmer and P. Bennema, J. Appl. Phys. **43**, 1347 (1972).
[25] A. Karma and M. Plapp, Phys. Rev. Lett. **81**, 4444 (1998).
[26] A. C. Levi and M. Kotrla, J. Phys.: Condens. Matter **9**, 299 (1997).
[27] Y. Lou and P. D. Christofides, Chem. Eng. Sci. **58**, 3115 (2003).
[28] V. Cheng, E. Tang, and T. Tang, J. Cryst. Growth **96**, 293 (1989).
[29] W. Cai, V. V. Bulatov, S. Yip, and A. S. Argon, Mater. Sci. Eng. A **309**, 270 (2001).
[30] D. A. McQuarrie, J. Appl. Prob. **4**, 413 (1967).
[31] D. T. Gillespie, J. Phys. Chem. **81**, 2340 (1977).
[32] A. E. Blum and A. C. Lasaga, in *Aquatic Surface Chemistry*, edited by W. Stumm (Wiley, New York, 1987).
[33] P. Meakin, P. Ramanlal, L. M. Sander, and R. C. Ball, Phys. Rev. A **34**, 5091 (1986).
[34] P. Meakin and R. Jullien, Phys. Rev. A **41**, 983 (1990).
[35] L. Zhang and A. Luttge, Am. Mineral. **92**, 1316 (2007).
[36] A. Luttge, R. S. Arvidson, and C. Fischer, Elements **9**, 183 (2013).
[37] K. A. Fichthorn and W. H. Weinberg, J. Chem. Phys. **95**, 1090 (1991).
[38] J. J. Lukkien, J. P. L. Segers, P. A. J. Hilbers, R. J. Gelten, and A. P. J. Jansen, Phys. Rev. E **58**, 2598 (1998).
[39] S. M. Ross, *Simulation* (Academic, Amsterdam, 2013).
[40] S. L. Brantley and N. Mellott, Am. Mineral. **85**, 1767 (2000).
[41] D. Farin and D. Avnir, J. Phys. Chem. **91**, 5517 (1987).
[42] J. C. Arnault, A. Knoll, E. Smigiel, and A. Cornet, Appl. Surf. Sci. **171**, 189 (2001).
[43] Chunfang Fan and H. H. Teng, Chem. Geol. **245**, 242 (2007).
[44] H. H. Teng, P. Fenter, L. Cheng, and N. C. Sturchio, Geochim. Cosmochim. Acta **65**, 3459 (2001).
[45] S. Brunauer, P. H. Emmett, and E. Teller, J. Am. Chem. Soc. **60**, 309 (1938).
[46] A. F. White and M. L. Peterson, in *Chemical Modeling of Aqueous Systems II*, edited by D. C. Melchior and R. L. Bassett (American Chemical Society, Washington, DC, 1990), p. 461.
[47] A. Luttge, Am. Mineral. **90**, 1776 (2005).
[48] S. L. Brantley, A. F. White, and M. Hodson, in *Growth and Dissolution in Geosystems*, edited by B. Jamtveit and P. Meakin (Kluwer Academic, Dordrecht, 1999), p. 291.
[49] H. C. Helgeson, W. M. Murphy, and P. Aagard, Geochim. Cosmochim. Acta **48**, 2405 (1984).
[50] P. Pfeifer, D. Avnir, and D. Farin, Surf. Sci. **126**, 569 (1983).
[51] P. M. Dove and F. M. Platt, Chem. Geol. **127**, 331 (1996).
[52] H. H. Teng, P. M. Dove, and J. J. D. Yoreo, Geochim. Cosmochim. Acta **64**, 2255 (2000).
[53] N. P. Mellott, S. L. Brantley, and C. G. Pantano, in *Water-Rock Interactions, Ore Deposits, and Environmental Geochemistry, A Tribute to David A. Crerar*, edited by R. Hellmann and S. Wood (The Geochemical Society, St. Louis, MO, 2002), p. 83.
[54] P. H. Dumas, B. Bouffakhreddine, C. Amra, O. Vatel, E. Andre, R. Galindo, and F. Salvan, Europhys. Lett. **22**, 717 (1993).
[55] P. Gollion and G. Grenet, Surf. Interface Anal. **24**, 282 (1996).
[56] D. L. Turcotte, *Fractals and Chaos in Geology and Geophysics*, 2nd ed. (Cambridge University Press, Cambridge, 1997).
[57] E. Aharonov and D. H. Rothman, J. Geophys. Res. **101**, 2973 (1996).
[58] O. Vatel, P. H. Dumas, F. Chollet, F. Salvan, and E. Andre, Jpn. J. Appl. Phys. **32**, 5671 (1993).
[59] I. Okuda and N. Senesi, in *Structure and Surface Reactions of Soil Particles*, edited by P. M. Huang, N. Senesi, and J. Buffle (Wiley, Chichester, 1998), p. 78.
[60] A. K. Navarre-Sitchler, D. Cole, G. Rother, L. Jin, H. L. Buss, and S. L. Brantley, Geochim. Cosmochim. Acta **109**, 400 (2013).
[61] E. Bazilevskaya, G. Rother, D. Mildner, M. Pavich, D. Cole, M. Bhatt, L. Jin, C. Steefel, and S. L. Brantley (unpublished).
[62] R. S. Sayles and T. R. Thomes, Nature (London) **271**, 431 (1978).
[63] R. J. Glauber, J. Math. Phys. **4**, 294 (1963).
[64] A. C. Lasaga and A. Luttge, Eur. J. Mineral. **15**, 603 (2003).